Assimilation of Disaggregated Microwave Soil Moisture into a Hydrologic Model Using Coarse-Scale Meteorological Data

O. MERLIN, A. CHEHBOUNI, G. BOULET, AND Y. KERR

Centre d'Etudes Spatiales de la Biosphère, Toulouse, France

(Manuscript received 24 October 2005, in final form 28 April 2006)

ABSTRACT

Near-surface soil moisture retrieved from Soil Moisture and Ocean Salinity (SMOS)-type data is downscaled and assimilated into a distributed soil–vegetation–atmosphere transfer (SVAT) model with the ensemble Kalman filter. Because satellite-based meteorological data (notably rainfall) are not currently available at finescale, coarse-scale data are used as forcing in both the disaggregation and the assimilation. Synthetic coarse-scale observations are generated from the Monsoon '90 data by aggregating the Push Broom Microwave Radiometer (PBMR) pixels covering the eight meteorological and flux (METFLUX) stations and by averaging the meteorological measurements. The performance of the disaggregation/assimilation coupling scheme is then assessed in terms of surface soil moisture and latent heat flux predictions over the 19-day period of METFLUX measurements. It is found that the disaggregation improves the assimilation results, and vice versa, the assimilation of the disaggregated microwave soil moisture improves the spatial distribution of surface soil moisture at the observation time. These results are obtainable regardless of the spatial scale at which solar radiation, air temperature, wind speed, and air humidity are available within the microwave pixel and for an assimilation frequency varying from 1/1 day to 1/5 days.

1. Introduction

Rainfall and soil moisture are key variables of the terrestrial hydrosphere. Whereas rainfall provides the amount of available water at the surface, soil moisture controls the partitioning of rainfall into runoff and infiltration and the incident energy into sensible and latent heat flux. The knowledge of both complementary variables is hence critical for achieving efficient and sustainable water management and for improvements in climate change prediction.

Both variables are characterized by strong variabilities in space and time (Rodriguez-Iturbe et al. 1995; Famiglietti et al. 1999). Because of these variabilities and because many surface processes are nonlinearly related to rainfall and soil moisture, the representation of hydrological processes at the model scale needs to account for the surface heterogeneity at finescale. Following the terminology of Giorgi and Avissar (1997), the use of coarse-resolution data may have a "dynamical" impact on runoff predictions (Entekhabi and Eagleson 1989; Goodrich et al. 1994; Faures et al. 1995; Ghan et al. 1997; Goodrich et al. 1997; Yu et al. 1999) as well as an "aggregation impact" on surface fluxes (Famiglietti and Wood 1995; Wood 1997; Kustas and Norman 2000; Crow and Wood 2002). In this context, the spatial scale at which most hydrological processes (runoff, infiltration, evapotranspiration, etc.) should be captured for improving the understanding and subsequently the representation of surface processes in regional models has been recognized to range from 1 to 10 km (Entekhabi and Eagleson 1989; Famiglietti and Wood 1995; Wood 1997; Crow and Wood 2002).

Because satellite-based rainfall estimates at improved spatial and temporal resolutions are increasingly required for various environmental studies, new methods have been developed to combine multisatellite data (e.g., Huffman et al. 2001; Joyce et al. 2004). For example, the Precipitation Estimation from Remotely Sensed Information using Artificial Neural Networks algorithm (Hsu et al. 1997, 1999) is a merging method combining the low-frequency (1–2 per day) but relatively accurate Tropical Rainfall Measuring Mission (TRMM) radar data with the high-frequency (48 per day) thermal infrared data provided by geosynchronous

Corresponding author address: Dr. Oliver Merlin, Centre d'Etudes Spatiales de la Biosphère, 18 avenue Edouard Belin, CEDEX 9, Toulouse 31401, France.
E-mail: merlin@cesbio.cnes.fr

© 2006 American Meteorological Society

satellites. Although the temporal resolution of the rainfall products obtained with merging methods is very attractive, the spatial resolution is still too coarse for a direct use of such data into distributed hydrological models. In fact, the rainfall data derived from the cloud-top temperature obtained in the thermal infrared are generally aggregated to reduce errors. This limits the spatial resolution of the current satellite-based rainfall products to about 0.25° (30 km) (Sorooshian et al. 2000).

Assimilation strategies of the surface soil moisture estimated from microwave data have been found to be an operational tool for controlling land surface–atmosphere interactions during interstorm periods (e.g., Crow and Wood 2003; Reichle and Koster 2005). In particular, the analysis of Crow (2003) has successfully tested the ability of the assimilation of surface brightness temperature observations to correct land surface model predictions for the impact of low-frequency rainfall measurements. However, these studies circumvented horizontal-scale issues either by using a climatic-scale grid size (>50 km) or higher-resolution airborne soil moisture imagery. The main limitation of the monodimensional assimilation of passive microwave soil moisture for hydrological applications is the poor resolution obtained with the current and near-future microwave-based satellite data (10 to 40 km) (Jackson et al. 1999).

To bridge the gap between the resolution of the surface soil moisture derived from passive microwave data (about 40 km) and the input scale required for hydrological applications (about 1 km), a variety of methods have been developed to improve the resolution of passive microwave data. They use either statistical correlations between surface soil moisture (or brightness temperature) and finescale auxiliary data as in Bindlish and Barros (2002), Kim and Barros (2002), and Chauhan et al. (2003) or distributed physically based models in conjunction with finescale auxiliary data as in Pellenq et al. (2003) and Merlin et al. (2005). The coupling of such methods with an assimilation scheme of the surface soil moisture is expected to provide significant improvements in the representation of vertical and horizontal hydrological processes.

The disaggregation method of Merlin et al. (2005) uses thermal and optical data remotely sensed at a typical resolution of 1 km to estimate the subpixel variability of microwave soil moisture. A relationship between soil skin temperature and surface soil moisture is developed at finescale to estimate a distribution as a function of two parameters defined at the microwave scale. Both parameters are then sequentially inverted from multi-independent (at least two independent) microwave observations. The requirement of multi-independent/multiangular observations is notably met by the Soil Moisture and Ocean Salinity (SMOS) (Kerr et al. 2001) mission, which is based on a radiometer at L band with significant angular viewing configurations.

In this paper, SMOS-type data are disaggregated with the method of Merlin et al. (2005) and assimilated into a distributed (with a typical resolution of 1 km) soil–vegetation–atmosphere transfer (SVAT) model with the ensemble Kalman filter (Evensen 1994). As the current spatial resolution of global-scale precipitation data is about the same as for passive microwave data, rainfall is assumed to be available at the microwave resolution (40 km). The objective is to assess the use of a disaggregation/assimilation coupling scheme of microwave data to compensate errors in terms of surface soil moisture and latent heat flux associated with the use of coarse-scale rainfall data only.

The analysis is based on a synthetic dataset generated from the Monsoon '90 data (Kustas and Goodrich 1994). The strategy adopted to test the downscaling/assimilation procedure is to

- calibrate a SVAT and a brightness temperature model against the Monsoon '90 observations;
- create synthetic soil skin temperature and SMOS observations based on calibrated model runs;
- perturb synthetic observations;
- downscale synthetic SMOS observations;
- assimilate downscaled synthetic observations;
- compare to the Monsoon '90 observations.

Note that the 5-cm soil moisture observations are used both to generate synthetic observations and to validate the assimilation/downscaling procedure. This approach thus parallels a traditional synthetic experiment in all regards except that it substitutes observed soil moisture for model-generated (model-dependent) soil moisture.

The Monsoon '90 data, the models, and the methods are successively presented in sections 2, 3, and 4. In section 5, the models are calibrated against the Monsoon '90 data and a synthetic dataset is generated. In section 6, the disaggregation/assimilation coupling scheme is applied to the synthetic dataset and assimilation results are compared to ground soil moisture measurements.

2. The Monsoon '90 data

The Monsoon '90 experiment was conducted during the summer of 1990 over the U.S. Department of Agriculture Agricultural Research Service (USDA-ARS) Walnut Gulch Experimental Watershed (WGEW) in

southeastern Arizona (Kustas et al. 1991; Kustas and Goodrich 1994). The purpose of the experiment was to observe the moisture fluxes in a semiarid climate during a dry-down and the role of remote sensing in determining these fluxes. A network of eight meteorological surface energy flux (METFLUX) stations covering the main study area (about 150 km^2) were situated in grass-dominated and shrub-dominated ecosystems and in the transition zones containing both vegetation types. The data collected at each METFLUX site from Julian day (JD) 204 to JD 222 consist of 20-min estimates of 0–5-cm soil moisture, meteorological conditions at screen height composed of air temperature, relative humidity, wind speed and solar radiation, surface fluxes composed of net radiation, soil heat flux measured at −5 cm, sensible heat flux, and latent heat flux.

As part of the Monsoon '90 campaign, the National Aeronautics and Space Administration (NASA) Push Broom Microwave Radiometer (PBMR) was flown on six flights of the C-130 aircraft during a 10-day period in July and August of 1990 (Schmugge et al. 1994). The objective was to map the surface brightness temperature at a wavelength of 21 cm (L band) and to infer surface soil moisture from these data. The four beams of PBMR point at ±8° and ±24° incidence angle with a 3-dB beamwidth of about 30% of the altitude. For Monsoon '90 the PBMR flights were at an altitude of 600 m, which yielded an instantaneous field of view (FOV) of 180 m. Available PBMR data of the Monsoon '90 experiment are nadir brightness temperatures. To create the images of the brightness temperature at nadir, the outer beams were corrected for incidence angle effects by multiplying them by the ratio of the average of the inner beam to the outer beam on each side (Schmugge et al. 1994).

3. Models

A SVAT and an empirical brightness temperature model are presented in this section.

a. ICARE

The Interactive Canopy Radiation Exchange (ICARE) SVAT model (Gentine et al. 2006) is dedicated to simulate the heat, mass, and momentum exchange within the continuum soil–vegetation–atmosphere over continental surfaces. The climate forcing is composed of the incoming shortwave radiation R_s (W m^{-2}), air temperature T_a (°C), wind speed u_a (m s^{-1}), relative humidity of air q_a (%), and precipitation P (mm). The surface state is a vector composed of the surface soil moisture W (%), the deep soil moisture W_2 (%), the soil surface temperature T (K), and the deep soil temperature T_2 (K).

The evolution of soil temperature follows the force-restore model proposed by Deardorff (1978):

$$\begin{cases} \dfrac{\partial T}{\partial t} = c_1 \dfrac{G}{\rho_s c_s (\lambda_s \tau)^{1/2}} - c_2 \dfrac{T - T_2}{\tau} \\ \dfrac{\partial T_2}{\partial t} = \dfrac{G}{\rho_s c_s (365 \lambda_s \tau)^{1/2}} \end{cases}, \tag{1}$$

where G is the conduction in the soil, ρ_s is the soil density, c_s is the soil specific heat, λ_s is the soil thermal conductivity, and c_1, c_2 are two parameters computed for each period of 1-day τ.

The evolution of the soil moisture content is described following the force–restore formulation using two soil layers as proposed in Interactions between Soil, Biosphere, and Atmosphere (ISBA; Noilhan and Planton 1989):

$$\begin{cases} \dfrac{\partial W}{\partial t} = C_1 \dfrac{P - \mathrm{LE}_s}{\rho_w d_1} - C_2 \dfrac{W - W_{\mathrm{eq}}}{\tau} & \text{while } 0 < W < W_{\mathrm{fc}} \\ \dfrac{\partial W_2}{\partial t} = \dfrac{P - \mathrm{LE}_s - \mathrm{LE}_c}{\rho_w d_2} & \text{while } 0 < W_2 < W_{\mathrm{fc}} \end{cases}, \tag{2}$$

where LE_s is the soil evaporation, LE_c is the vegetation transpiration, W_{eq} is an equivalent moisture for the restore effect on the surface moisture due to the root zone moisture, W_{fc} is the moisture at field capacity, C_1, C_2 are two parameters, d_1 is the depth of the surface layer, d_2 is the mean depth of the deep layer, and ρ_w is the water density. Parameters C_1, C_2 and W_{fc} are estimated using the pedotransfer functions of Noilhan and Mahfouf (1996) and sand and clay fractions.

ICARE uses the common dual-source formulation by Shuttleworth and Wallace (1985) and its network of resistances. The aerodynamic resistances for heat and water vapor are computed as in Choudhury and Monteith (1988). The bulk stomatal resistance is expressed as the product of a minimum stomatal resistance and four stress functions (Jarvis 1976). The soil resistance to evaporation r_{ss} is expressed as in Camillo and Gurney (1986):

$$r_{\mathrm{ss}} = \exp(A - BW/W_{\mathrm{fc}}), \tag{3}$$

where A and B are two calibration parameters.

b. An empirical brightness temperature model

An empirical brightness temperature (EBT) model is used to simulate the L-band brightness temperatures remotely sensed by the PBMR instrument during the Monsoon '90 experiment. Over the 10-day period of PBMR observations, Schmugge et al. (1994) found no correlation of the variation of the slopes of the relation between PBMR brightness temperature/ground-based soil moisture with any soil or vegetation parameters (e.g., sand, clay, percentage rock or biomass). In fact, the physically based tau-omega formalism (Mo et al. 1982; Brunfeldt and Ulaby 1984; Ulaby et al. 1986) could not be used to model the L-band surface emission. However, the results of Schmugge et al. (1994) on a site-by-site basis indicated excellent correlation of PBMR brightness temperatures with ground-based soil moisture. In this study, the results of Schmugge et al. (1994) are therefore used to build an empirical relationship between PBMR data and ground soil moisture measurements.

The formulation of the angular brightness temperature TB^{α} simulated by the EBT model at the incidence angle α is given by

$$TB^{\alpha} = a^{\alpha}W^2 + b^{\alpha}W + c^{\alpha}, \tag{4}$$

where W is the 0–5-cm soil water content and a^{α}, b^{α}, and c^{α} are three angular parameters. The EBT model simulates the PBMR observation at 8° ($TB^{\perp}$) and 24° ($TB^{\angle}$) given the six parameters $\mathbf{X} = (a^{\perp}, b^{\perp}, c^{\perp}, a^{\angle}, b^{\angle}, c^{\angle})$.

Note that the quadratic fit of Eq. (4) based on the PBMR data of Monsoon '90 is not state of the art. The development of physically based radiative transfer models will actually be a critical step in the application to SMOS or other passive microwave data.

4. Methods

The disaggregation method and the ensemble Kalman filter are presented in this section.

a. Disaggregation method

The disaggregation method is fully described in Merlin et al. (2005). Basically, soil skin temperature observations are combined with the modeling of land surface–atmosphere interactions to estimate a spatial distribution of surface soil moisture within the microwave pixel. The distribution is then calibrated at the scale of the microwave pixel with a SMOS-type multiangular observation.

1) ESTIMATE A DISTRIBUTION

The spatial variability of surface soil moisture within the microwave pixel is explained by the soil skin temperature retrieved from fine-resolution optical/thermal data. Because soil skin temperature depends on surface variables other than surface soil moisture (e.g., soil texture, solar radiation, etc.), a SVAT model is used to remove the influence of finescale surface parameters and meteorological data on soil skin temperature. In this study, ICARE predictions are used to estimate the impact (noted ΔT^{SVAT}) of the variability of surface parameters (vector $\mathbf{Y}$) and meteorological data (vector $\mathbf{Z}$) on soil skin temperature:

$$\Delta T^{\mathrm{SVAT}} = \mathrm{ICARE}(W, \mathbf{Y}, \mathbf{Z}) - \mathrm{ICARE}(W, \langle \mathbf{Y} \rangle, \langle \mathbf{Z} \rangle), \tag{5}$$

where ICARE predictions are the soil skin temperatures solved by the energy budget, $\langle \mathbf{Y} \rangle$ is the vector of the surface parameters averaged at the microwave scale, and $\langle \mathbf{Z} \rangle$ is the vector of the meteorological variables averaged at the microwave scale. A variable called "projected soil temperature" and denoted $\overline{T}$ is then computed as

$$\overline{T} = T - \Delta T^{\mathrm{SVAT}}, \tag{6}$$

where T is the measured soil skin temperature. The projected soil temperature is the variable to be used by the disaggregation method to estimate the spatial variability of surface soil moisture within the microwave pixel. In practice, the disaggregated soil moisture W^{disag} is expressed at first order as function of the projected soil temperature:

$$W^{\mathrm{disag}} = W_{\mathrm{SMOS}} + f_1(\overline{T} - \langle \overline{T} \rangle), \tag{7}$$

where $\langle \overline{T} \rangle$ is the average of the finescale projected soil temperature, W_{SMOS} is the microwave-scale soil moisture, and f_1 is a first-order coefficient fixing the range covered by downscaled values.

2) CALIBRATE THE DISTRIBUTION

Both parameters W_{SMOS} and f_1 of Eq. (7) are inverted from a SMOS-type observation. In practice, a cost function F is first built to evaluate the distance between simulated and measured microwave observations:

$$F(W_{\mathrm{SMOS}}, f_1) = \| \langle \mathrm{EBT}(W^{\mathrm{disag}}, \mathbf{X}) \rangle - \mathbf{TB_{SMOS}} \|^2, \tag{8}$$

where $\langle \mathrm{EBT}(W^{\mathrm{disag}}, \mathbf{X}) \rangle$ is the average within the SMOS pixel of the finescale simulated observation and $\mathbf{TB_{SMOS}}$ is the measured observation. The cost function F is then minimized sequentially to invert the microwave-scale soil moisture $W^{\mathrm{inv}}_{\mathrm{SMOS}}$:

$$W^{\mathrm{inv}}_{\mathrm{SMOS}} = \mathrm{Min}_{W_{\mathrm{SMOS}}} F(W_{\mathrm{SMOS}}, 0) \tag{9}$$

and the first-order coefficient f_1^{inv}:

$$f_1^{\text{inv}} = \text{Min}_{f_1} F(W_{\text{SMOS}}^{\text{inv}}, f_1). \quad (10)$$

At this point, all the downscaled values of (7) are determined.

b. Ensemble Kalman filter

The Ensemble Kalman (EnK) filter (Evensen 1994) is used to assimilate the downscaled soil moisture into ICARE. The EnK filter has the advantage of being relatively simple to implement and computationally efficient compared to other filters like the extended Kalman filter (Evensen 1992). It is based on the generation of an ensemble of model predictions to estimate the covariance information required by the standard Kalman filter for the updating of model predictions with observations. Covariance information is calculated by propagating in time the ensemble of state vectors and by averaging at the time of measurement the predictions made by model replicates within the ensemble. In the study, the state vector is noted $\mathbf{S} = (W, W_2, T, T_2)$ and is always defined at finescale.

As finescale soil skin temperature T is used as input to the disaggregation method, it is also assimilated into the SVAT model at the same time as the downscaled soil moisture W^{disag}. Both variables W^{disag} and T are correlated because W^{disag} is retrieved from the spatial distribution of T. But T does provide some independent information on the surface state S because W^{disag} is obtained with a combination of two independent observations, which are T and TB_{SMOS}. In particular, the assimilation of T (in addition to W^{disag}) can compensate some errors in W^{disag} associated with uncertainties in SMOS observation. The observation vector to be assimilated at finescale is noted $\mathbf{O} = (W^{\text{disag}}, T)$.

An ensemble of N initial state vectors $\mathbf{S}_{t_0}^{i=1\ldots N}$ is computed from a normal distribution with a mean equal to the guess and covariance equal to the estimated uncertainties on the variables. These N points are propagated in time until an observation is available. At the time of measurement, the vector of observations $\mathbf{O}$ is used to generate a set of N observation vectors $\mathbf{O}_{t>t_0}^{m,i=1\ldots N}$ from a normal distribution of variance equal to the estimated observation uncertainty. For each point of the ensemble, the state variables are then readjusted, according to the uncertainties of observed data and of simulated variables. If the model is linear and all errors are additive, independent, and Gaussian, the optimal updating of ICARE predictions $\mathbf{S}^{s,i}$ by the measurement $\mathbf{O}^{m,i}$ is given by

$$\mathbf{S}_{t_k}^{a,i} = \mathbf{S}_{t_k}^{s,i} + \mathbf{K}_k(\mathbf{O}_{t_k}^{m,i} - \mathbf{O}_{t_k}^{s,i}), \quad (11)$$

where $\mathbf{S}^{a,i}$ is the analyzed state vector after readjustment and $\mathbf{O}^{s,i}$ the simulated observation. The expression of the Kalman gain K_k that minimizes the analyzed error covariance is given by

$$\mathbf{K}_k = \{\mathbf{C}_{\mathbf{S}^s\mathbf{O}^s}(\mathbf{C}_{\mathbf{O}^s} + \mathbf{C}_{\mathbf{O}})^{-1}\}_{t_k}, \quad (12)$$

where $\mathbf{C}_{\mathbf{S}^s\mathbf{O}^s} = \langle(\mathbf{S}^{s,i} - \mathbf{S}^s)(\mathbf{O}^{s,i} - \mathbf{O}^s)^{\text{T}}\rangle$ is the cross-covariance matrix linking the predicted observations with the predicted state variables, $\mathbf{C}_{\mathbf{O}^s} = \langle(\mathbf{O}^{s,i} - \mathbf{O}^s)(\mathbf{O}^{s,i} - \mathbf{O}^s)^{\text{T}}\rangle$, the error covariance matrix of the measurement forecasts, and $\mathbf{C}_{\mathbf{O}} = \langle(\mathbf{O}^{m,i} - \mathbf{O})(\mathbf{O}^{m,i} - \mathbf{O})^{\text{T}}\rangle$, the error covariance matrix of the measured observations.

5. Synthetic data

Synthetic SMOS pixels, which are subject to disaggregation, are generated by aggregating the PBMR pixels covering the eight METFLUX sites. The EBT model and ICARE are calibrated against the Monsoon '90 data, and calibrated model runs are used to generate synthetic coarse-scale biangular microwave observations and synthetic finescale soil skin temperature observations over the 19-day period JD 204–222. Synthetic coarse-scale meteorological observations are generated by averaging the measurements at the eight METFLUX sites. Such a synthetic dataset is finally perturbed to account for the uncertainty in observations.

a. Synthetic coarse-scale SMOS observations

The EBT model is calibrated against the Monsoon '90 observations at the eight METFLUX sites. Ground soil moisture measurements are inserted into the EBT model and simulated brightness temperatures are compared to PBMR data. Parameters $a^{\perp}$, $b^{\perp}$, and $c^{\perp}$ are evaluated by minimizing the root-mean-square (RMS) difference between the EBT generated and measured nadir brightness temperature at each METFLUX site. The results of Schmugge et al. (1994) are used to calibrate parameters $a^{\perp}$, $b^{\perp}$, and $c^{\perp}$. Schmugge et al. (1994) estimated the angular effects of PBMR data by computing the ratio of the average of the inner beam to the average of the outer beam on each side of the instrument, and on each day of PBMR observations. In this study, a PBMR oblique brightness temperature is first simulated by dividing the Monsoon '90 nadir brightness temperature by the same ratios as in Schmugge et al. (1994). Parameters $a^{\angle}$, $b^{\angle}$, and $c^{\angle}$ are then evaluated by minimizing the root-mean-square difference between the EBT-generated and PBMR-simulated oblique

TABLE 1. Calibration parameters of ICARE and the EBT model at the eight METFLUX sites.

Site	A	B	$a^{\perp}$	$b^{\perp}$	$c^{\perp}$	$a^{\angle}$	$b^{\angle}$	$c^{\angle}$
1	8	8	0.14	−10.14	330.38	0.21	−11.75	333.40
2	7	4	−0.024	−2.65	298.41	−0.020	−2.93	296.14
3	8	7	0.062	−5.79	305.72	0.080	−6.46	304.99
4	8	6	0.14	−7.46	332.50	0.16	−8.17	333.55
5	8	7	−0.25	1.40	298.19	−0.25	0.91	299.97
6	8	7	0.0075	−6.67	326.60	0.031	−7.57	328.00
7	7	4	−0.26	0.97	276.30	−0.24	0.41	273.26
8	7	6	0.017	−3.55	292.77	0.027	−3.96	290.19

brightness temperatures. Calibration parameters are listed in Table 1.

The nadir brightness temperature simulated by the calibrated EBT model versus the Monsoon '90 nadir brightness temperature is plotted in Fig. 1. The root-mean-square error on the simulated nadir brightness temperature is found to be 4 K. Figure 1 also illustrates the angular dependency of the simulated brightness temperature to surface soil moisture: for wetter days the ratio of the average of the inner beam to the outer beam is about 1.03 and for dry days the ratio is about 1.01.

A synthetic SMOS observation $\mathbf{TB_{SMOS}} = (\langle TB^{\perp} \rangle, \langle TB^{\angle} \rangle)$ is generated every day at 12 A.M by simulating the microwave emission at the eight METFLUX sites with the calibrated EBT model and by averaging the eight nadir and the eight oblique simulated brightness temperatures.

b. *Synthetic finescale soil skin temperature observations*

ICARE is calibrated against latent heat flux observations. All the surface parameters are fixed to the homogeneous values used in Houser et al. (1998) for the WGEW. Parameters A and B are estimated at the eight METFLUX sites by fixing the water status (W and W_2) and by minimizing the root-mean-square difference between the simulated and measured latent heat flux. Given that root-zone soil moisture is available at two METFLUX sites only (Kendall and Lucky Hills), a mean value of 15% is taken for the simulation. Calibration parameters are listed in Table 1 and results are presented in Table 2. Figure 2 illustrates the simulated latent heat flux for the time period JD 204–222 (only positive fluxes are considered). Note that the issue here is not to validate the model but rather to make sure that ICARE is realistic.

The calibrated energy budget model of ICARE is used to generate the synthetic finescale soil skin temperature at 12 A.M. by inserting the observations of 5-cm soil moisture and meteorological forcings.

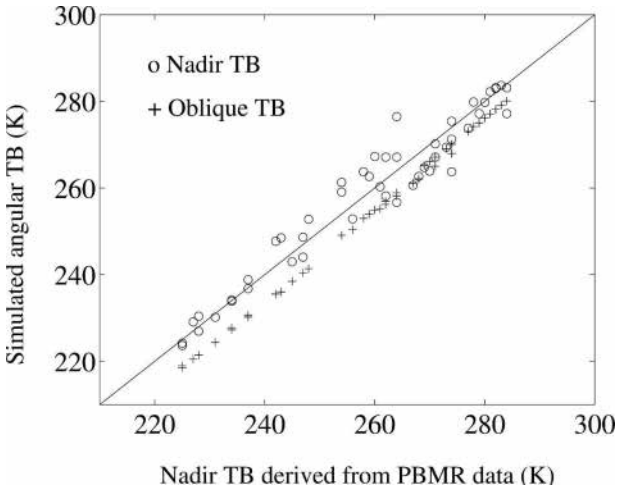

FIG. 1. Angular brightness temperature simulated by the EBT model vs the Monsoon '90 nadir brightness temperature.

c. *Synthetic coarse-scale meteorological observations*

1) RAINFALL

The current spatial resolution of global-scale precipitation data is still too coarse to be used at the input scale required for hydrological applications. To account for this limitation, coarse-scale precipitation data are generated by averaging the measurements at the eight METFLUX stations.

2) OTHER METEOROLOGICAL VARIABLES

Different cases are considered for the other meteorological variables. In the dataset METEO1, all the atmospheric forcing variables composed of solar radiation, air temperature, wind speed, and air humidity are assumed to be available at finescale (model scale). In the dataset METEO2, solar radiation is assumed to be available at finescale and the other variables (air temperature, wind speed, and air humidity) at coarse scale (microwave resolution). In the dataset METEO3, all

TABLE 2. Results of the calibration of ICARE over the eight METFLUX sites.

	RMS error (W m^{-2}) on			
Site	Net radiation	Ground heat flux	Sensible heat flux	Latent heat flux
1	31	30	30	40
2	28	31	29	38
3	29	30	34	45
4	33	40	36	48
5	39	40	36	50
6	31	35	32	37
7	37	38	29	41
8	47	42	35	42

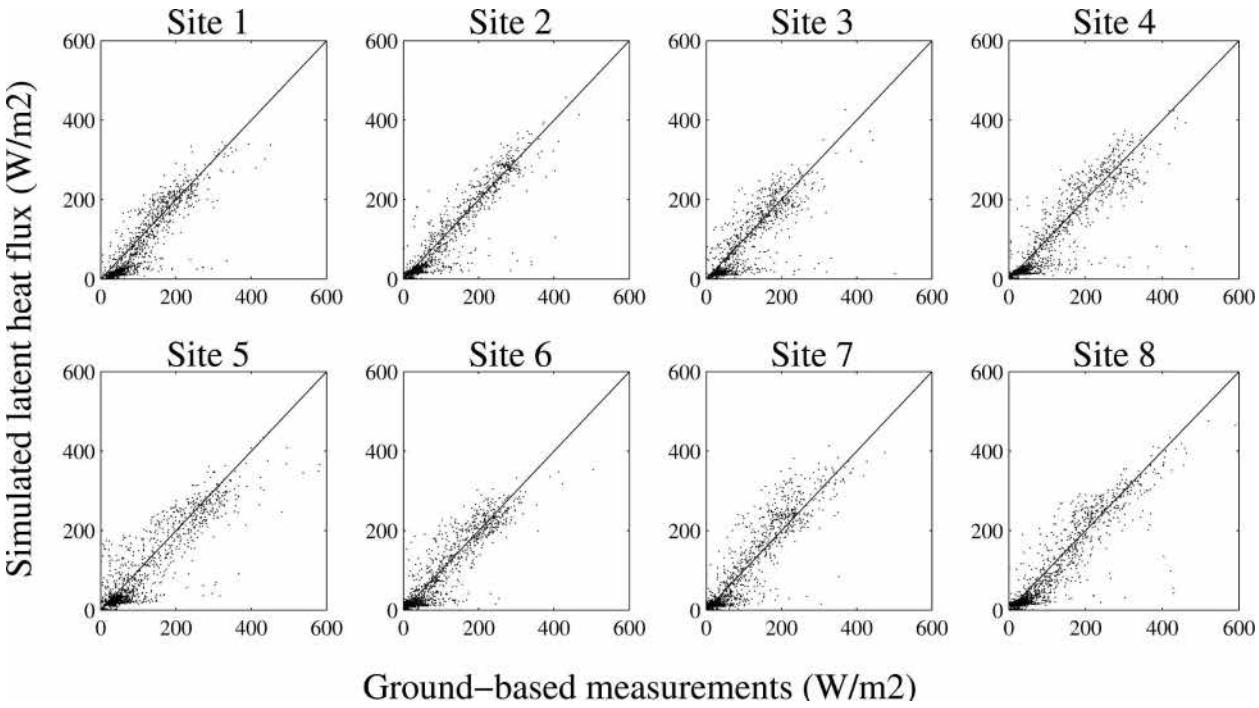

FIG. 2. Latent heat flux simulated by ICARE vs ground-based measurements at the eight METFLUX sites.

the meteorological variables are available at coarse scale only. Coarse-scale meteorological variables are generated by averaging the finescale meteorological data.

d. Perturb synthetic observations

A spatially uncorrelated Gaussian noise of 4 K is added to the generated finescale brightness temperature (4 K is the standard deviation found between simulated and measured nadir brightness temperatures). A spatially uncorrelated Gaussian noise of 1 K is added to the generated finescale soil skin temperature. A noise equal to the standard deviation observed within the SMOS pixel is added to the aggregated rainfall (negative values are set to zero). A noise of 1 K and 10% of the measured value is systematically added to respectively finescale ground-based air temperature and finescale ground-based solar radiation, wind speed, and air humidity. A noise equal to the standard deviation observed within the SMOS pixel is added to the meteorological variables generated at the microwave scale.

6. Application

The disaggregation method is applied to the synthetic dataset, and downscaled synthetic observations are assimilated into ICARE with the ensemble Kalman filter. The objective is to assess the ability of the disaggregation/assimilation coupling scheme to correct errors associated with the use of meteorological data (including rainfall) estimated at coarse scale only. The impact of the assimilation frequency is also investigated.

a. Disaggregation

The disaggregation method is applied to the time series of synthetic SMOS pixels. Each day of the 19-day period, the algorithm is run 50 times on the randomly noised dataset generated at 12 A.M. and composed of synthetic coarse-scale SMOS observation, synthetic finescale soil skin temperature observations, and the meteorological forcings at either fine- or coarse scale depending on the dataset used (METEO1, -2, and -3). The 50 separate replicates are used to compute the mean and standard deviation of the downscaled surface soil moisture within the ensemble.

The downscaled surface soil moisture is compared to ground measurements in Fig. 3 (first line). The subgrid variability of surface soil moisture is generally well represented in the case of METEO1. In particular, parameters $W_{\mathrm{SMOS}}^{\mathrm{inv}}$ and f_1^{inv} appear to be retrieved with a satisfying accuracy from synthetic SMOS observations.

If the datasets METEO1 and -2 are compared, it is apparent that the heterogeneity of air temperature, wind speed, and air humidity has not a significant impact. However, the much noisier results with the dataset METEO3 indicate that solar radiation is the atmospheric variable whose finescale variability affects the most the downscaled soil moisture.

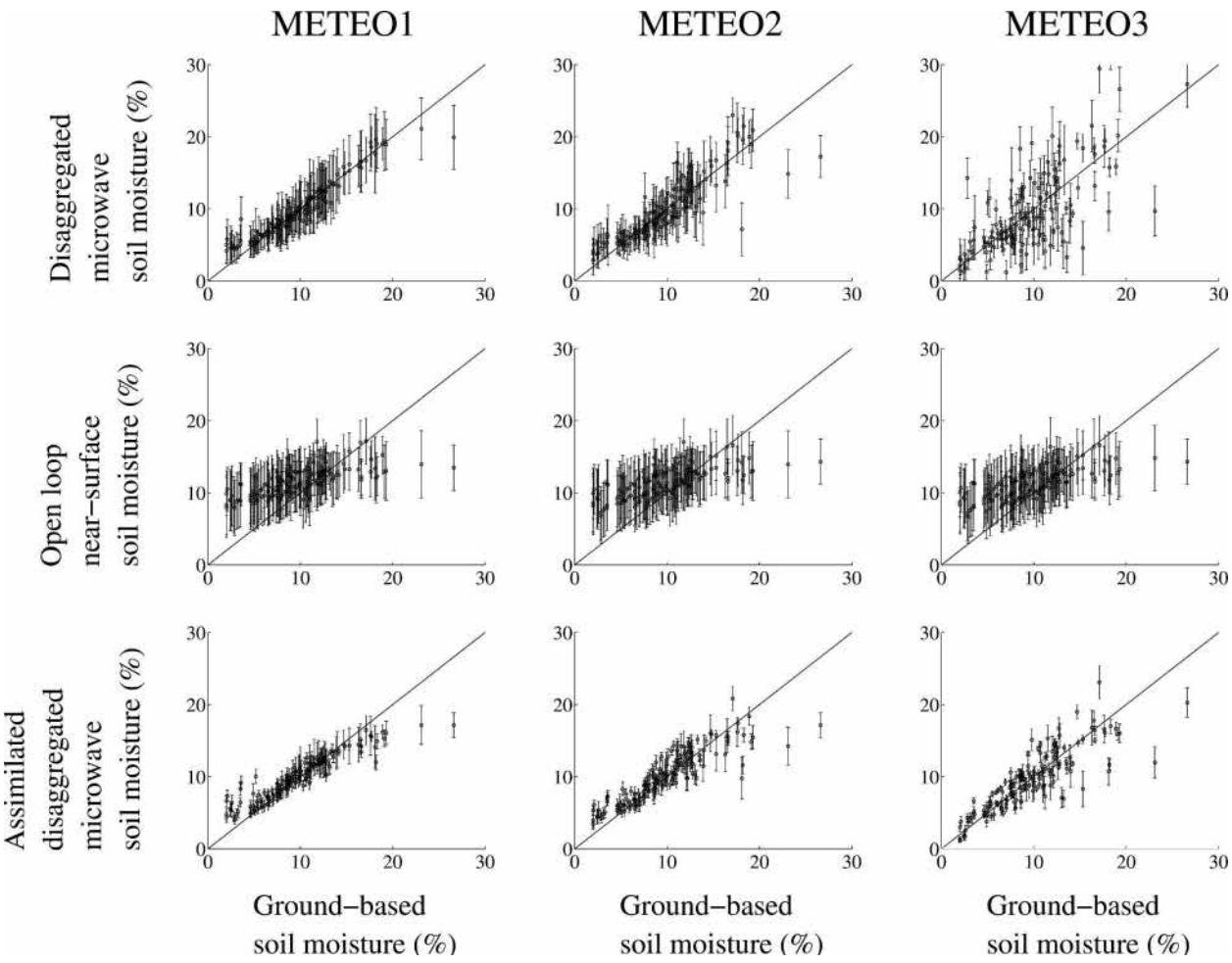

FIG. 3. Mean (circles) and std dev (error bars) of the surface soil moisture simulated by the disaggregation method, ICARE in open loop, and the disaggregation–assimilation coupling scheme. Statistical results were computed within an ensemble of 50 replicates.

In Table 3, the mean error on the downscaled soil moisture is compared to the average of solar radiation and its standard deviation within the SMOS pixel. In general, the error obtained with the datasets METEO1 and -2 is negatively correlated to the microwave-scale solar radiation. Note that the variability of solar radiation was mainly due to the presence of clouds, conditions for which the soil skin temperature is not available in an operational scenario, and the disaggregation method is not applicable. In fact, even if the application of the method for cloudy conditions (e.g., on JD 214) is an exercise in style, the sensitivity of the method to solar radiation can be tested.

Based on datasets METEO1 and -2, a saturation of the downscaled soil moisture is observed in Fig. 3 for low soil moisture values (<4%) as well as for relatively high values (>25%). This is due to the exponential formulation of the soil resistance r_{ss} in (3). By controlling the soil evaporation, the soil resistance parameterizes the correlation between soil skin temperature and surface soil moisture. The nonlinearities of the soil resistance thus impact the soil skin temperature, which in turn makes the downscaled soil moisture saturate.

b. *Assimilation of downscaled observations*

The downscaled surface soil moisture W^{disag} and synthetic finescale soil skin temperature T are both assimilated into ICARE with the EnK filter. The 50 separate replicates used in the disaggregation are now used to update the state vector every day at 12 A.M. Before the assimilation, the dependence in T and W^{disag} errors is removed by replacing each individual state vector by the mean vector of the 50-member ensemble and by adding a Gaussian noise equal to the standard deviation computed within the ensemble.

The state vector of the replicate i within the ensemble is initialized with $W^i_{t_0}$ and $W^i_{2,0}$ uniformly distributed between 5% and 20% and $T^i_{t_0}$ and $T^i_{2,0}$ distrib-

TABLE 3. RMS error on the downscaled surface soil moisture. Disaggregation results obtained with datasets METEO1, -2, and -3 are compared with the average of solar radiation and its std dev within the SMOS pixel.

	RMS error on the downscaled values (%)			Solar radiation (W m^{-2})
JD	METEO1	METEO2	METEO3	Average (std dev)
204	0.7	1.9	4.7	747 (89)
205	0.8	2.6	6.2	698 (105)
206	0.4	2.2	4.4	958 (95)
207	0.6	1.5	3.2	995 (12)
208	0.5	1.0	2.2	984 (11)
209	1.1	1.3	1.4	985 (10)
210	1.1	1.2	1.4	977 (9)
211	1.5	1.7	4.1	678 (79)
212	1.6	1.8	4.7	929 (102)
213	1.2	1.1	0.8	1042 (29)
214	2.2	6.3	8.5	760 (166)
215	0.4	2.3	7.0	906 (114)
216	0.9	2.1	3.4	794 (79)
217	0.5	1.5	3.0	929 (141)
218	2.1	2.2	4.0	216 (17)
219	1.0	1.6	6.9	743 (105)
220	1.2	1.2	2.6	810 (204)
221	1.7	1.3	1.9	922 (60)
222	1.4	1.1	1.6	957 (43)

uted by a Gaussian function with a standard deviation of 10 K and a mean of 300 K. Between two assimilations, the atmospheric data used as forcing at the eight METFLUX sites are estimated at either fine- or microwave scale, depending on the dataset used (METEO1, -2, or -3).

Figures 4 and 5 illustrate the EnK's sequential assimilation of the synthetic finescale observation (W^{disag}, T) with the dataset METEO1 (all the atmospheric variables except rainfall are provided at finescale) at the eight METFLUX sites. Surface soil moisture predictions compare better to ground measurements with the disaggregation/assimilation coupling scheme than with the "open loop," where ICARE is run from the initial guess without assimilation. Note that the open-loop surface soil moisture estimates appear to have a smaller dynamic range than the observations. This dynamic range error is mainly due to the fact that ICARE was not calibrated against surface soil moisture observations but against latent heat flux observations.

The comparison of disaggregation and assimilation results in Fig. 3 indicates that the assimilation generally improves the downscaled soil moisture. The coupled scheme therefore combines the spatial (but static) information provided by the disaggregation method with the temporal (but monodimensional) information provided by the assimilation scheme in an optimal way.

c. Impact of coarse-scale meteorological data

Figure 3 illustrates the impact of coarse-scale meteorological data by comparing the disaggregation and assimilation results obtained with datasets METEO1, -2, and -3. With datasets METEO2 and -3, the projection approach is not able to remove the meteorological influences on soil skin temperature T, which involves additional errors on the downscaled soil moisture W^{disag}. However, the assimilation results (with datasets METEO2 and -3) are relatively similar to those obtained with METEO1. It is suggested that the random errors on W^{disag} due to the meteorological influences on T are significantly reduced with the sequential assimilation process.

The comparison in Fig. 3 of the disaggregation and assimilation results obtained with the dataset METEO1 indicates that the assimilation makes the downscaled soil moisture saturate above 18%. The nonrepresentation of some local rainfall events (notably on JD 213 at METFLUX site 4) causes an underestimation of the highest surface soil moisture values.

d. Comparison with other assimilation schemes

To assess the utility of the disaggregation, the disaggregation/assimilation coupling scheme is compared to two other assimilation schemes: the assimilation of the synthetic finescale soil skin temperature T only and the assimilation at finescale of the synthetic observation ($W^{\text{inv}}_{\text{SMOS}}$, T). The dataset METEO1 is used in this application. Note that the assimilation of "T only" assumes an infinite uncertainty in microwave observations and that the microwave-scale soil moisture $W^{\text{inv}}_{\text{SMOS}}$ is retrieved with Eq. (9).

Figure 6 illustrates the temporal variation of the error on the surface soil moisture simulated by the open loop, the assimilation of T only, the assimilation of ($W^{\text{inv}}_{\text{SMOS}}$, T), and the assimilation of (W^{disag}, T). The microwave-scale error and the finescale error are respectively evaluated as the average and the standard deviation of the finescale biases within the SMOS pixel. The finescale biases are computed as the average between 10 A.M. and 5 P.M. of the difference between the predicted and measured surface soil moisture.

The comparison of the assimilation of "T only" (Fig. 6b) with the open loop (Fig. 6a) indicates that the assimilation of soil skin temperature is able to reduce the error on surface soil moisture at both fine- and microwave scales. In Fig. 6c, it is apparent that the assimilation of the microwave-scale soil moisture (in addition to soil skin temperature) significantly improves the predictions at the microwave scale but degrades the estimations at finescale. The comparison of the assimilation of

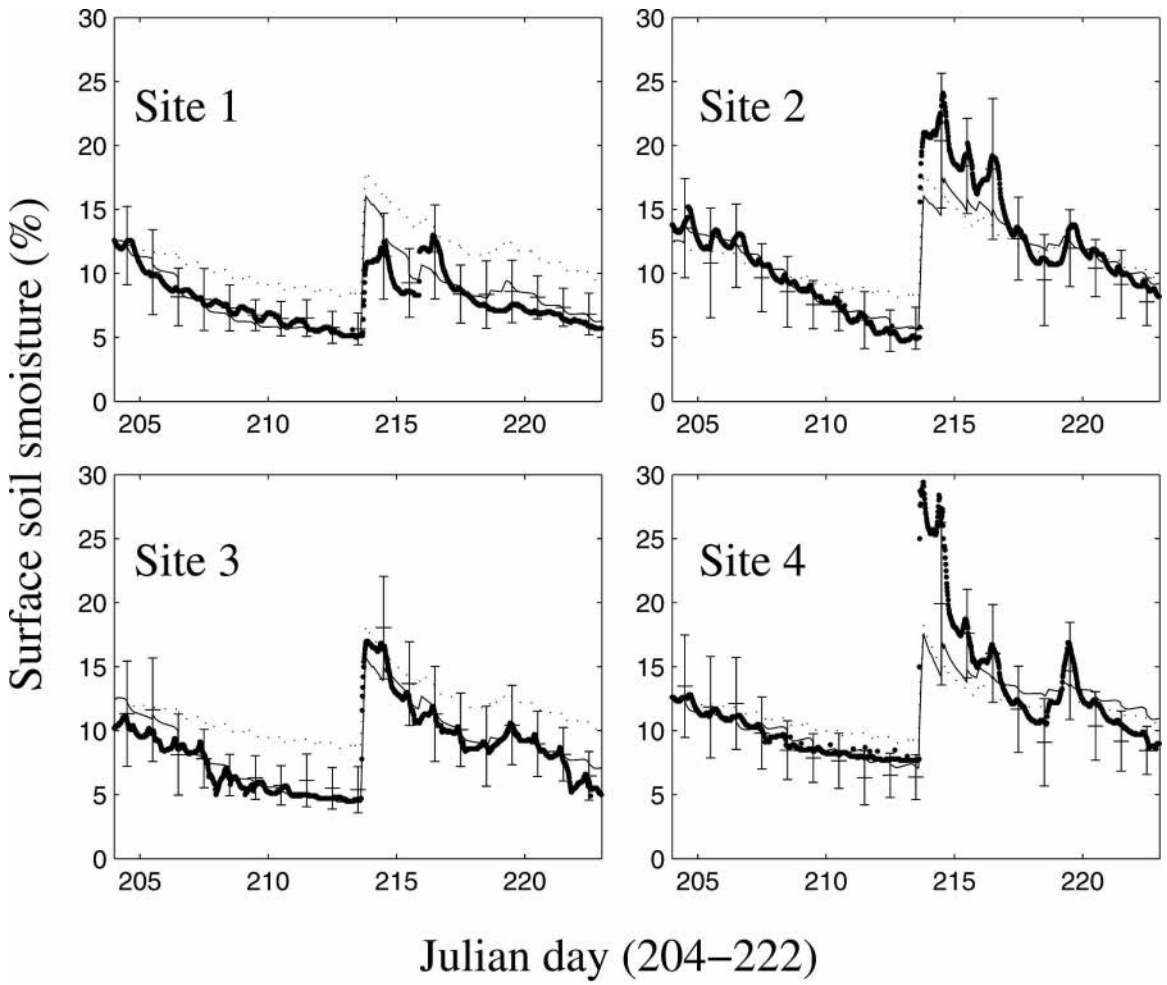

FIG. 4. Temporal variations for sites 1 to 4 of the measured 0–5-cm soil moisture (thick dotted line), the downscaled surface soil moisture (the mean and standard deviation within the ensemble are represented), the surface soil moisture simulated by ICARE with the assimilation of (W^{disag}, T) (continuous line represents the mean within the ensemble), and the surface soil moisture simulated by ICARE in open loop (dotted line represents the mean within the ensemble).

(W^{disag}, T) with the assimilation of ($W^{\text{inv}}_{\text{SMOS}}$, T) indicates that the disaggregation improves the estimation of surface soil moisture at finescale (the width of error bars is reduced in Fig. 6d) but not at the microwave scale. Finally, the comparison of the assimilation of (W^{disag}, T) with the assimilation of "T only" shows that the changes in the updates are mainly driven by surface soil moisture observations. The long-term memory of surface soil moisture (compared to soil skin temperature) is actually accounted for in the Kalman gain.

Because the disaggregation of microwave data is expected to improve surface fluxes, the performance of the disaggregation/assimilation coupling scheme is also evaluated in terms of latent heat flux predictions. Figure 7 illustrates the temporal variation of the error on the latent heat flux simulated by the open loop, the assimilation of T only, the assimilation of ($W^{\text{inv}}_{\text{SMOS}}$, T), and the assimilation of (W^{disag}, T). It is found that the disaggregation generally improves latent heat flux predictions at finescale, and also at the microwave scale except in two periods. During JD 213–216, the assimilation of (W^{disag}, T) is less efficient at the microwave scale than the assimilation of ($W^{\text{inv}}_{\text{SMOS}}$, T) because the (unresolved) spatial variability of rainfall is relatively high and the frequency of rainfall events is higher than the assimilation frequency. In the period JD 221–222, the errors on latent heat flux are mainly due to the overestimation of the downscaled soil moisture at METFLUX site 7.

e. Impact of the assimilation frequency

The assimilation frequency is decreased from 1/1 day to 1/5 days to assess its impact on the assimilation results. The disaggregation/assimilation coupling scheme

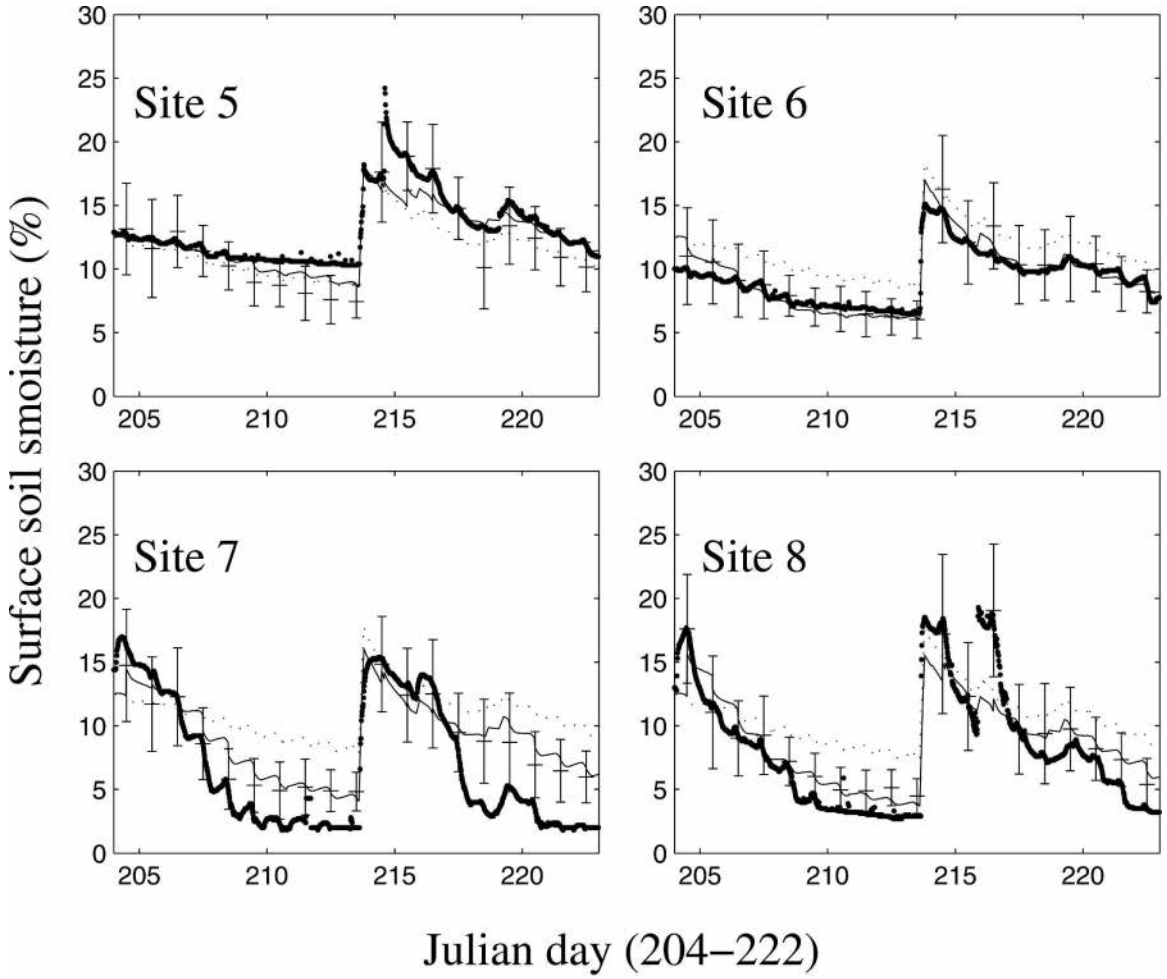

FIG. 5. Temporal variations for sites 5 to 8 of the measured 0–5-cm soil moisture (thick dotted line), the downscaled surface soil moisture (the mean and standard deviation within the ensemble are represented), the surface soil moisture simulated by ICARE with the assimilation of (W^{disag}, T) (continuous line represents the mean within the ensemble), and the surface soil moisture simulated by ICARE in open loop (dotted line represents the mean within the ensemble).

can hence be tested with an assimilation frequency consistent with future microwave-based missions. Note that the frequency of SMOS will be of about 2–3 days depending on the latitude of the pixel.

The assimilation schemes of (W^{disag}, T) and of ($W^{\text{inv}}_{\text{SMOS}}$, T) are run with the dataset METEO1 for three different assimilation frequencies: 1/1 day, 1/3 days, and 1/5 days. The results are compared by evaluating the average and the standard deviation within the SMOS pixel of the mean error between JD 204 and JD 222 on the finescale surface soil moisture. Because the 19-day period is not long enough to assess the performance of the assimilation strategies with an assimilation frequency ranging from 1/5 days to 1/3 days, three different cases are considered for the assimilation frequency 1/3 days and five different cases are considered for the assimilation frequency 1/5 days by incrementing the first date of assimilation of 1 day. For example, three results are computed with the assimilation frequency 1/3 days corresponding respectively to the three possible first assimilation dates: JD 204, JD 205, or JD 206.

Table 4 illustrates the effect of a decreasing assimilation frequency on the performance of the approach in terms of surface soil moisture predictions. Even if the efficiency of the assimilation naturally depends on the timing of assimilation dates with rainfall events, the coupled disaggregation/assimilation behaves generally better than the assimilation of the microwave-scale surface soil moisture regardless of the assimilation frequency and the first date of assimilation.

7. Conclusions

Near-surface soil moisture retrieved from synthetic SMOS data is downscaled with the method of Merlin et

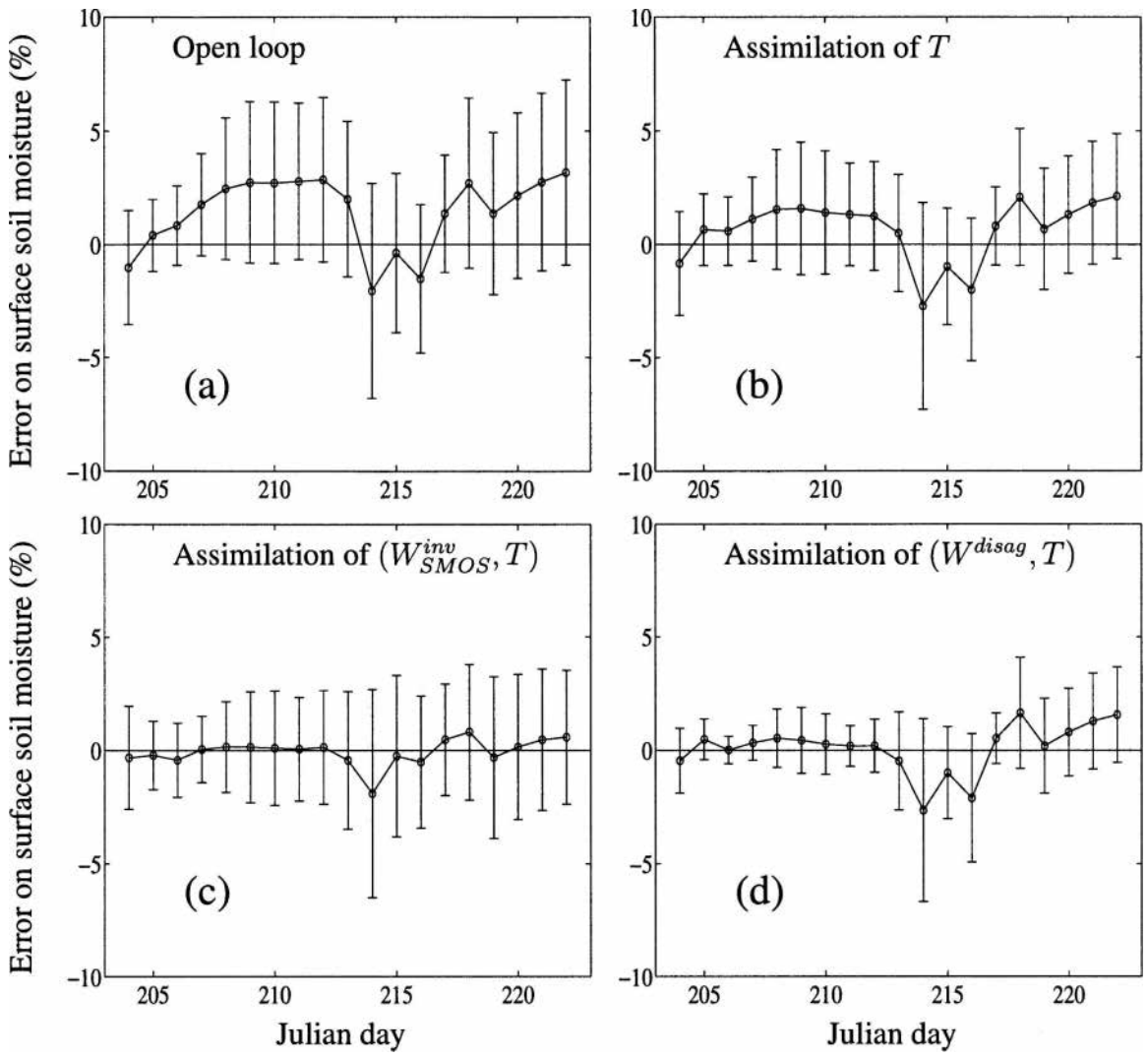

FIG. 6. Error on the surface soil moisture simulated by ICARE in (a) open loop, (b) the assimilation of T, (c) the assimilation of ($W^{\text{inv}}_{\text{SMOS}}$, T), and (d) the assimilation of (W^{disag}, T). The microwave-scale error (circles) and the finescale error (error bars) are respectively evaluated as the average and the standard deviation of the finescale biases within the SMOS pixel. The finescale biases are computed as the average between 10 A.M. and 5 P.M. of the difference between the predicted and measured surface soil moisture.

al. (2005) and assimilated into a distributed land surface model with the ensemble Kalman filter. Because satellite-based meteorological data (notably rainfall) are not currently available at finescale, coarse-scale data are used as forcing in both the disaggregation and the assimilation. The objective is to assess the use of a disaggregation/assimilation coupling scheme to compensate errors in terms of surface soil moisture and latent heat flux associated with the use of meteorological data at coarse scale only. The strategy adopted to test the approach is to calibrate a land surface and a brightness temperature model against the Monsoon '90 data, create synthetic data from calibrated model runs, apply the disaggregation/assimilation, and compare to real observations.

The application of the disaggregation method to coarse-scale and/or finescale meteorological data indicates that solar radiation is the most important variable to be estimated at finescale. In particular, the spatial variability of air temperature, wind speed, and air humidity has a minor impact on downscaled values. Downscaled synthetic observations are then assimilated into the distributed land surface model. It is found that the disaggregation improves the assimilation results in terms of surface soil moisture predictions, and vice versa, the assimilation of the downscaled soil moisture

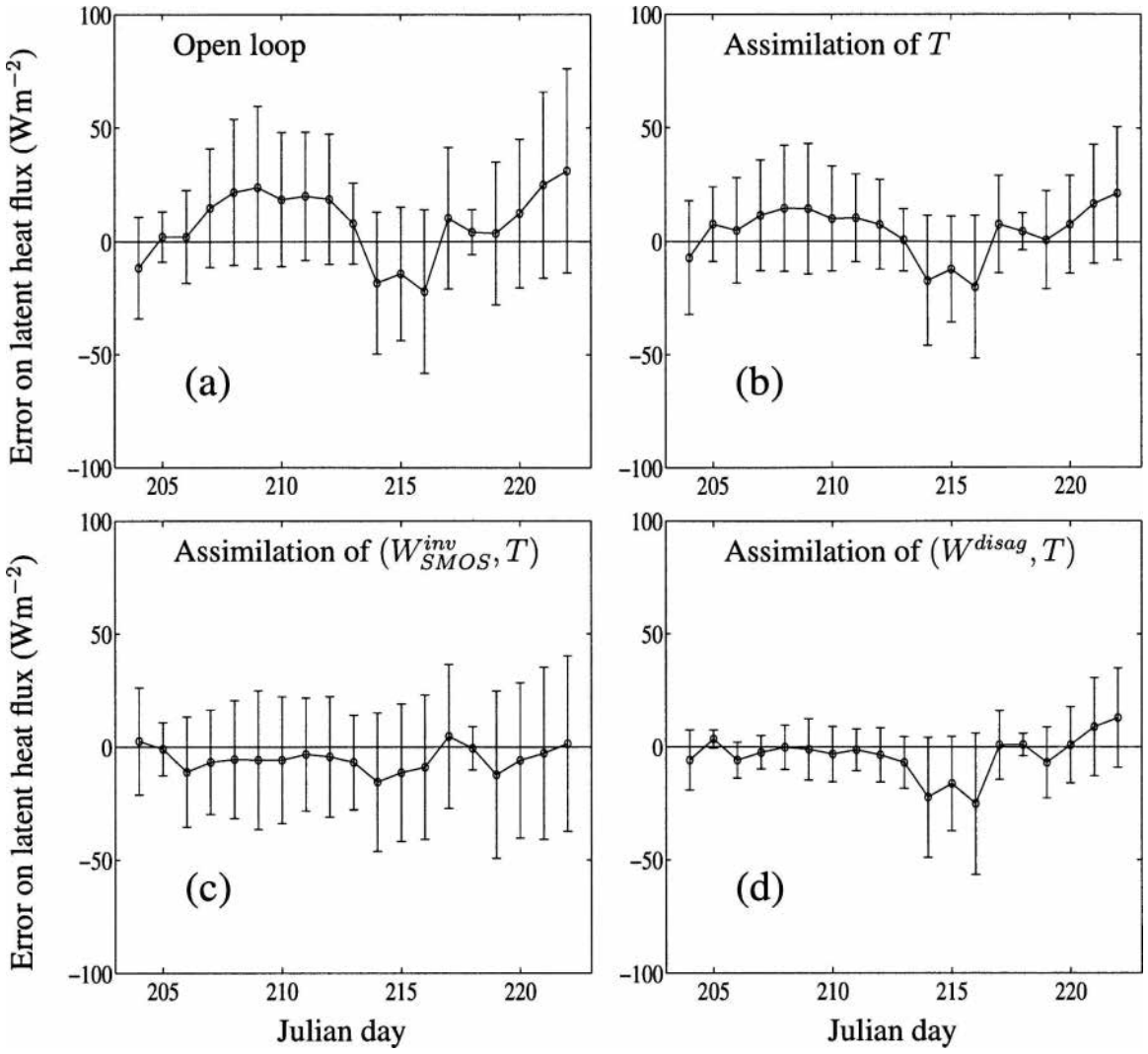

FIG. 7. Error on the latent heat flux simulated by ICARE in (a) open loop, (b) the assimilation of T, (c) the assimilation of (W^{inv}_{SMOS}, T), and (d) the assimilation of (W^{disag}, T). The microwave-scale error (circles) and the finescale error (error bars) are respectively evaluated as the average and the standard deviation of the finescale biases within the SMOS pixel. The finescale biases are computed as the average between 10 A.M. and 5 P.M. of the difference between the predicted latent heat flux and the latent heat flux of reference simulated by ICARE with the direct insertion of ground measurements.

improves the spatial distribution of surface soil moisture at the observation time. Latent heat flux predictions are subsequently improved, at both fine- and microwave scales. The use of coarse-scale rainfall data in the assimilation has the effect of underestimating the highest values of surface soil moisture. Because of the nonrepresentation of some local rainfall events, the assimilated–disaggregated soil moisture saturates to a threshold estimated with these data and model parameters to about 18%. Finally, the disaggregation–assimilation coupling scheme is tested with a decreasing assimilation frequency from 1/1 day to 1/5 days. It is found that the assimilation of the disaggregated soil moisture still behaves significantly better than both the open-loop system (no assimilation) and the assimilation of the microwave-scale soil moisture.

These encouraging results show that the disaggregation of passive microwave soil moisture is able to improve the representation of the surface processes occurring at both fine- and microwave scales, even when coarse-scale meteorological data including rainfall are used. However, the 19-day period used in the paper is very short and longer periods should be used in the future to assess the robustness of the approach. Moreover, the error sources were perfectly known in this study. The application to real data will require accurate

TABLE 4. Average over the 19-day period of the error on the finescale surface soil moisture simulated by the open loop, the assimilation of (W^{inv}_{SMOS}, T), and the assimilation of (W^{disag}, T). The mean and the std dev of the error within the SMOS pixel are presented for an assimilation frequency decreasing from 1/1 day to 1/5 days.

		Error on surface soil moisture (%)		
		Open loop	Without disaggregation	With disaggregation
Frequency	First date	Mean (std dev)	Mean (std dev)	Mean (std dev)
1/1 day	JD204	1.4 (2.4)	−0.07 (2.1)	0.09 (0.92)
1/3 days	JD204	1.4 (2.4)	0.19 (2.2)	0.13 (1.1)
	JD205	1.4 (2.4)	−0.19 (2.1)	0.10 (1.1)
	JD206	1.4 (2.4)	−0.24 (2.1)	−0.10 (1.1)
1/5 days	JD204	1.4 (2.4)	0.23 (2.0)	0.25 (1.3)
	JD205	1.4 (2.4)	−0.07 (2.1)	0.14 (1.1)
	JD206	1.4 (2.4)	0.27 (2.2)	0.20 (1.5)
	JD207	1.4 (2.4)	−0.23 (2.1)	0.02 (1.2)
	JD208	1.4 (2.4)	−0.31 (2.1)	−0.11 (1.4)

characterization of the uncertainty in input data, notably the rainfall data. One should also note that this study took place in a very arid region where the coupling between surface temperature and surface soil moisture is relatively strong. The physical basis of the downscaling approach would be weakened in areas where surface evaporation is energy limited.

Optical data are not available for cloudy days but microwave data still provide information on surface soil moisture. If the disaggregation method used in the paper is not strictly applicable for cloudy conditions, the finescale surface soil moisture simulated by a distributed land surface model could still be constrained by adjusting the mean level of the predicted distribution to the microwave-scale soil moisture.

In the case of multivariable data assimilation, further studies have to focus on the impact of the relative uncertainties in the observation variables (e.g., surface soil moisture and surface temperature). Assimilation results may be sensitive to the relative weight attributed to those variables, especially when they are observed at different spatial resolutions.

Acknowledgments. The authors thank William Kustas, David Goodrich, Susan Moran, and Tom Schmugge for making the Monsoon '90 data available. In addition, the past and current support of the USDA-ARS-SWRC staff in Tombstone and Tucson are gratefully acknowledged. The necessary financial support to conduct the Monsoon '90 field experiment is also acknowledged. This included funds from NASA Interdisciplinary Research Program in Earth Sciences (NASA Reference IDP-88-086) and funds from the USDA-ARS Beltsville Area Office. This work was supported by a grant from CNES and CNRS and the CNES program TOSCA.

REFERENCES

Bindlish, R., and A. R. Barros, 2002: Subpixel variability of remotely sensed soil moisture: An inter-comparison study of SAR and ESTAR. *IEEE Trans. Geosci. Remote Sens.,* **40,** 326–337.

Brunfeldt, D. R., and F. T. Ulaby, 1984: Measured microwave emission and scattering in vegetation canopies. *IEEE Trans. Geosci. Remote Sens.,* **22,** 520–524.

Camillo, P. J., and R. J. Gurney, 1986: A resistance parameter for bare soil evaporation models. *Soil Sci.,* **141,** 95–105.

Chauhan, N. S., S. Miller, and P. Ardanuy, 2003: Spaceborne soil moisture estimation at high resolution: A microwave-optical/IR synergistic approach. *Int. J. Remote Sens.,* **24,** 4599–4622.

Choudhury, B. J., and J. L. Monteith, 1988: A four-layer model for the heat budget of homogeneous land surfaces. *Quart. J. Roy. Meteor. Soc.,* **114,** 373–398.

Crow, W. T., 2003: Correcting land surface model predictions for the impact of temporally sparse rainfall rate measurements using an ensemble Kalman filter and surface brightness temperature observations. *J. Hydrometeor.,* **4,** 960–973.

——, and E. F. Wood, 2002: The value of coarse-scale soil moisture observations for regional surface energy balance modeling. *J. Hydrometeor.,* **3,** 467–482.

——, and ——, 2003: The assimilation of remotely sensed soil brightness temperature imagery into a land surface model using ensemble Kalman filtering: A case study based on ESTAR measurements during SGP97. *Adv. Water Resour.,* **26,** 137–149.

Deardorff, J., 1978: Efficient prediction of ground surface temperature and moisture, with inclusion of a layer of vegetation. *J. Geophys. Res.,* **83,** 1889–1903.

Entekhabi, D., and P. S. Eagleson, 1989: Land surface hydrology parameterization for atmospheric general circulation models including subgrid scale spatial variability. *J. Climate,* **2,** 816–831.

Evensen, G., 1992: Using the extended Kalman filter with a multilayer quasi-geostrophic ocean model. *J. Geophys. Res.,* **97,** 17 905–17 924.

——, 1994: Sequential data assimilation with a nonlinear quasi-geostrophic model using Monte Carlo methods to forecast error statistics. *J. Geophys. Res.,* **99,** 10 143–10 162.

Famiglietti, J. S., and E. F. Wood, 1995: Effects of spatial variabil-

ity and scale on areally averaged evapotranspiration. *Water Resour. Res.,* **31,** 699–712.

——, and Coauthors, 1999: Ground-based investigation of soil moisture variability within remote sensing footprints during the Southern Great Plains 1997 (SGP97) hydrology experiment. *Water Resour. Res.,* **35,** 1839–1851.

Faures, J. M., D. C. Goodrich, D. A. Woolhiser, and S. Sorooshian, 1995: Impact of small-scale spatial rainfall variability on runoff simulation. *J. Hydrol.,* **173,** 309–326.

Gentine, P., D. Entekhabi, A. Chehbouni, G. Boulet, and B. Duchemin, 2006: Analysis of diurnal evaporative fraction behavior. *Extended Abstracts, 20th Conf. on Hydrology,* Atlanta, GA, Amer. Meteor. Soc., CD-ROM, 1.12.

Ghan, S. J., J. C. Liljegren, W. J. Shaw, J. H. Hubbe, and J. C. Doran, 1997: Influence of subgrid variability on surface hydrology. *J. Climate,* **10,** 3157–3166.

Giorgi, F., and R. Avissar, 1997: Representation of heterogeneity effects in earth system modeling: Experience from land surface modeling. *Rev. Geophys.,* **35,** 413–438.

Goodrich, D. C., T. J. Schmugge, T. J. Jackson, C. L. Unkrich, T. O. Keefer, R. Parry, L. B. Bach, and S. A. Amer, 1994: Runoff simulation sensitivity to remotely sensed initial soil water content. *Water Resour. Res.,* **30,** 1393–1405.

——, L. J. Lane, R. A. Shillito, S. N. Miller, K. H. Syed, and D. A. Woolhiser, 1997: Linearity of basin response as a function of scale in a semi-arid watershed. *Water Resour. Res.,* **33,** 2951–2965.

Houser, P. R., W. J. Shuttleworth, H. V. Gupta, J. S. Famiglietti, K. H. Syed, and D. C. Goodrich, 1998: Integration of soil moisture remote sensing and hydrologic modeling using data assimilation. *Water Resour. Res.,* **34,** 3405–3420.

Hsu, K. L., X. Gao, S. Sorooshian, and H. V. Gupta, 1997: Precipitation estimation from remotely sensed information using artificial neural networks. *J. Appl. Meteor.,* **36,** 1176–1190.

——, H. V. Gupta, X. Gao, and S. Sorooshian, 1999: Estimation of physical variables from multichannel remotely sensed imagery using neural networks: Application to rainfall estimation. *Water Resour. Res.,* **35,** 1605–1618.

Huffman, G. J., R. R. Adler, M. M. Morrissey, D. T. Bolvin, S. Curtis, R. Joyce, B. McGavock, and J. Susskind, 2001: Global precipitation at one-degree daily resolution from multisatellite observations. *J. Hydrometeor.,* **2,** 36–50.

Jackson, T. J., D. M. L. Vine, A. Y. Hsu, A. Oldak, P. J. Starks, C. T. Swift, J. D. Isham, and M. Haken, 1999: Soil moisture mapping at regional scales using microwave radiometry: The Southern Great Plains Hydrology Experiment. *IEEE Trans. Geosci. Remote Sens.,* **37,** 2136–2151.

Jarvis, P., 1976: The interpretation of leaf water potential and stomatal conductance found in canopies in the field. *Philos. Trans. Roy. Soc. London,* **273,** 593–610.

Joyce, R., J. E. Janowiak, P. A. Arkin, and P. Xie, 2004: CMORPH: A method that produces global precipitation estimates from passive microwave and infrared data at high spatial and temporal resolution. *J. Hydrometeor.,* **5,** 487–503.

Kerr, Y. H., P. Waldteufel, J.-P. Wigneron, J.-M. Martinuzzi, J. Font, and M. Berger, 2001: Soil moisture retrieval from space: The soil moisture and ocean salinity (SMOS) mission. *IEEE Trans. Geosci. Remote Sens.,* **39,** 1729–1735.

Kim, G., and A. P. Barros, 2002: Downscaling of remotely sensed soil moisture with a modified fractal interpolation method using contraction mapping and ancillary data. *Remote Sens. Environ.,* **83,** 400–413.

Kustas, W. P., and D. C. Goodrich, 1994: Monsoon '90 multidisciplinary experiment. *Water Resour. Res.,* **30,** 1211–1225.

——, and J. M. Norman, 2000: Evaluating the effects of subpixels heterogeneity on pixel average fluxes. *Remote Sens. Environ.,* **74,** 327–342.

——, and Coauthors, 1991: An interdisciplinary field study of the energy and water fluxes in the atmosphere–biosphere system over semiarid rangelands: Description of some preliminary results. *Bull. Amer. Meteor. Soc.,* **72,** 1683–1705.

Merlin, O., G. Chehbouni, Y. Kerr, E. G. Njoku, and D. Entekhabi, 2005: A combined modeling and multi-spectral/multi-resolution remote sensing approach for disaggregation of surface soil moisture: Application to SMOS configuration. *IEEE Trans. Geosci. Remote Sens.,* **43,** 2036–2050.

Mo, T., B. J. Choudhury, T. J. Schmugge, J. R. Wang, and T. J. Jackson, 1982: A model for microwave emission from vegetation-covered fields. *J. Geophys. Res.,* **87,** 11 229–11 237.

Noilhan, J., and S. Planton, 1989: A simple parameterization of land surface processes for meteorological models. *Mon. Wea. Rev.,* **117,** 536–549.

——, and J.-F. Mahfouf, 1996: The ISBA land surface parameterisation scheme. *Global Planet. Change,* **13,** 145–159.

Pellenq, J., J. Kalma, G. Boulet, G.-M. Saulnier, S. Wooldridge, Y. Kerr, and A. Chehbouni, 2003: A disaggregation scheme for soil moisture based on topography and soil depth. *J. Hydrol.,* **276,** 112–127.

Reichle, R. H., and R. D. Koster, 2005: Global assimilation of satellite surface soil moisture retrievals into the NASA Catchment land surface model. *Geophys. Res. Lett.,* **32,** L02404, doi:10.1029/2004GL021700.

Rodriguez-Iturbe, I., G. K. Vogel, R. Rigon, D. Entekhabi, F. Castelli, and A. Rinaldo, 1995: On the spatial organization of soil moisture fields. *Geophys. Res. Lett.,* **22,** 2757–2760.

Schmugge, T., T. J. Jackson, W. P. Kustas, R. Roberts, R. Parry, D. C. Goodrich, S. A. Amer, and M. A. Weltz, 1994: Push broom microwave radiometer observations of surface soil moisture in Monsoon '90. *Water Resour. Res.,* **30,** 1321–1327.

Shuttleworth, W. J., and J. S. Wallace, 1985: Evaporation from sparse crops—An energy combination theory. *Quart. J. Roy. Meteor. Soc.,* **111,** 839–855.

Sorooshian, S., K. Hsu, X. Gao, H. V. Gupta, B. Imam, and D. Braithwaite, 2000: Evaluation of PERSIANN system satellite-based estimates of tropical rainfall. *Bull. Amer. Meteor.,* **81,** 2035–2046.

Ulaby, F. T., R. K. Moore, and A. K. Fung, 1986: *Microwave Remote Sensing—Active and Passive.* Vol. 3. Artech House, 1100 pp.

Wood, E. E., 1997: Effects of soil moisture aggregation on surface evaporation fluxes. *J. Hydrol.,* **190,** 397–412.

Yu, Z., and Coauthors, 1999: Simulation of the hydrologic response to atmospheric forcing in large river basins: Linking a mesoscale meteorological model and a hydrologic model system. *J. Hydrol.,* **218,** 72–91.